mater.scichina.com link.springer.com Published online 9 July 2021 | https://doi.org/10.1007/s40843-021-1708-6

Rapid CO_2 exfoliation of Zintl phase $CaSi_2$-derived ultrathin free-standing Si/SiO_x/C nanosheets for high-performance lithium storage

Lin Sun[1,2*], Jie Xie[1], Songchao Huang[1], Yanxiu Liu[1], Lei Zhang[1], Jun Wu[1] and Zhong Jin[1,2*]

ABSTRACT Semiconducting silicon (Si) nanomaterials have great potential for the applications in electronics, physics, and energy storage fields. However, to date, it is still a challenge to realize the batch production of Si nanomaterials *via* efficient and low-cost approaches, owing to some long-standing shortcomings, e.g., complex procedures and time and/or energy consumption. Herein, we report a green and inexpensive method to rapidly obtain two-dimensional (2D) free-standing Si/SiO_x nanosheets *via* the rapid thermal exfoliation of layered Zintl compound $CaSi_2$. With the help of the rapid exfoliation reaction of $CaSi_2$ in the atmosphere of greenhouse gas CO_2, and the following mild sonication, 2D free-standing Si/SiO_x nanosheets can be produced with very high yield. After applying the coating of a thin carbon outer layer, the electrodes of Si/SiO_x/C nanosheets serving as the anodes for lithium-ion batteries exhibit ultrahigh reversible capacity and outstanding electrochemical stability. We expect this study will provide new insights and inspirations for the convenient and batch production of nanostructural Si-based anode materials towards high-performance lithium-ion batteries.

Keywords: lithium-ion battery, two-dimensional silicon, anode, calcium silicide, greenhouse gas

INTRODUCTION

With the rapidly increasing demand for energy storage devices with high energy and power densities, it is of significant importance to discover and develop high-performance electrode materials for lithium-ion batteries (LIBs) [1–6]. In the past decade, silicon (Si)-based nanomaterials have been considered as one of the most promising alternative anode materials that may replace traditional graphite anode due to their ultrahigh specific capacity, abundance in the Earth, and relatively low working voltage [7–9]. However, both the issues of large volume expansion during the charge-discharge processes and the intrinsic poor conductivity of Si and SiO_x are still huge obstacles that hinder the development of Si-based anodes with high rate performance and long cycle lifetime [10–12].

In recent years, two-dimensional (2D) nanomaterials have been in the spotlight of research efforts since the discovery and development of emblematical graphene [13–15] and graphene-like 2D nanomaterials (e.g., transitional metal dichalcogenides (TMDs) [16–19], MXenes [20–24], h-BN [25,26] and g-C_3N_4 [27–29]). Because electrons are confined in ultrathin environments, 2D nanomaterials usually exhibit inimitable physical, electronic and chemical properties. When serving as an electrode material, Si with ultrathin 2D structures is expected as one of the most promising and effective anodes that will concurrently minimize the volume effects and accelerate electron migration [30–40]. Unfortunately, to date, rapid and efficient strategies to produce 2D Si and/or SiO_x nanomaterials in high yields are still lacking.

$CaSi_2$ is a layered Zintl compound in which the Ca and Si atomic layers are alternately stacked. Developing practical methods to exfoliate $CaSi_2$ is considered a hopeful route for the facile access to 2D Si nanomaterials. Most recently, several strategies have been proposed to break Ca–Si heteropolar bonds within the Zintl $CaSi_2$. For instance, concentrated acid etching at a low temperature (−30°C) was employed by Kumai *et al.* [41] to obtain 2D Si_6H_6 nanosheets. However, Si_6H_6 was not suitable to directly serve as an anode material in LIBs because of the limited lithium storage capacity (calculation reveals that the capacity contributions of the Si_6H_6 anode are merely rooted in the exchange of H and Li). Our previous work also developed a solvothermal method to prepare ultrathin SiO_x nanosheets in ionic liquids in the presence of ammonium salt [42]. It is worth noting that these existing methods usually have some shortcomings, such as rigorous reaction conditions with harsh temperature, low yield, long reaction time or environmental pollution. Accordingly, it is necessary to develop a convenient and environmentally friendly strategy to synthesize 2D Si-based nanomaterials.

In this work, combining the interaction between $CaSi_2$ and greenhouse gas CO_2 and the assistance of mild sonication, we developed an efficient and green process to rapidly obtain 2D free-standing Si/SiO_x nanosheets with ultrathin thickness of several nanometers. This method was environmentally friendly and it could significantly reduce the exfoliation reaction time. After coating with a thin carbon layer, the as-prepared Si/SiO_x/C nanosheets showed outstanding electrochemical stability when serving as an anodic electrode in LIBs. It delivered a high reversible specific capacity of ~1400 mA h g^{-1} at a current density of 0.1 A g^{-1}, and the capacity could be maintained even charging-discharging over 900 cycles. The superior electrochemcial performance could be attributed to the following

[1] School of Chemistry and Chemical Engineering, Yancheng Institute of Technology, Yancheng 224051, China
[2] MOE Key Laboratory of Mesoscopic Chemistry, MOE Key Laboratory of High Performance Polymer Materials and Technology, Jiangsu Key Laboratory of Advanced Organic Materials, Shenzhen Research Institute of Nanjing University, School of Chemistry and Chemical Engineering, Nanjing University, Nanjing 210023, China
* Corresponding authors (emails: sunlin@nju.edu.cn (Sun L); zhongjin@nju.edu.cn (Jin Z))

merits: (1) 2D ultrathin nanostructures with a large lateral size could effectively alleviate the stress induced by the volume expansion, and (2) the presence of SiO_x and carbon coatings is beneficial for the cycling stability and rate perfromance of the 2D Si anodes. It is believed that this work will provide new insights into the preparation of 2D Si-based nanomaterials that will attract widespread attention in the areas of materials science and high-energy batteries.

EXPERIMENTAL SECTION

Materials synthesis

Synthesis of ultrathin 2D Si/SiO$_x$ nanosheets

Briefly, commercial $CaSi_2$ powders (Sigma-Aldrich) were immersed into 2.0 mol L^{-1} aqueous NaOH solution and stirred at 600 rpm for 3 h at room temperature to dissolve any possible crystalline silicon impurities. The treated $CaSi_2$ was collected by centrifugation, washed with distilled water, and dried under vacuum for 4 h. The NaOH-treated $CaSi_2$ was placed in the center of a tube furnace and treated by a CO_2/Ar (1:4 in volume) gas flow at 700°C for 3 h. The volume flow rate of CO_2/Ar was ~100 mL min^{-1}, the inner diameter of the tube reactor was 45 mm, and the reaction was performed at atmospheric pressure. After the reaction, the formed dark-grey product was sonicated in dilute HCl solution and then distilled water to afford yellowish-brown production of ultrathin 2D Si/SiO_x nanosheets, and the conversion rate in terms of the utilization of Si atoms can be calculated as high as 95%.

Preparation of Si/SiO$_x$/C nanosheets

For carbon coating, the as-prepared Si/SiO_x nanosheets (0.4 g) were poured into tris-buffer (100 mL, 10 mmol L^{-1}) and sonicated for 5 min. Subsequently, 0.2 g of dopamine hydrochloride was added in the mixture, and the dispersion was further stirred for 10 h to induce the *in situ* polymerization of polydopamine on the surface of Si/SiO_x nanosheets. The product was collected and dried under vacuum. The dried sample was placed in a tube furnace and heated under high-purity Ar atomasphere at 400°C for 2 h with a heating rate of 2°C min^{-1}, and then at 800°C for 3 h with a heating rate of 5°C min^{-1} to yield black Si/SiO_x/C nanosheets. The pressure and Ar flow rate for the carbonization of the polydopamine coated on the Si/SiO_x nanosheets are close to the reaction condition between $CaSi_2$ and CO_2.

Characterizations

Powder X-ray diffraction (PXRD) data were collected on an X'Pert3 Powder instrument (PANalytical, Netherland) using a Cu Kα radiation at room temperature. Scanning electron microscopy (SEM) was conducted on a Nova NanoSEM 450 field-emission scanning electron microscope at an acceleration voltage of 15 kV. Transmission electron microscopy (TEM) and energy dispersive X-ray spectroscopy (EDS) were carried out using a JEM-1400-plus instrument (Japan). Atomic force microscopy (AFM) was conducted using a SPI3800/SPA400 instrument (Seiko Inc., Japan). Raman spectroscopy (InVia-Reflex, Renishaw) was performed with a laser source of 633 nm wavelength. X-ray photoelectron spectroscopy (XPS) data were recorded with an ESCALAB 250Xi (Thermo Fisher Scientific). Thermogravimetric analysis (TGA) was performed on a simultaneous STA449C thermal analyzer under flowing air with a heating rate of 5°C min^{-1}. Nitrogen adsorption/desorption isotherms were collected at 77 K (Micrometrics ASAP 2020 analyzer) after vacuum degassing of the sample at 200°C for 8 h.

Electrochemical measurements

CR2025 cells were assembled in an Ar-filled glove box to perform the electrochemical experiments. The electrode was composed of 80 wt% of active material, 10 wt% of conductive graphite, and 10 wt% of sodium carboxymethyl cellulose as a binder. The mixture was stirred in deionized water and blade-coated on a piece of Cu foil. After drying at 90°C in vacuum for 12 h, the foil was cut into disks of 12 mm in diameter. The electrolyte consisted of a solution of 1.0 mol L^{-1} $LiPF_6$ in a mixture of ethylene carbonate/diethyl carbonate (EC/DEC, 1:1 in volume) with 2 wt% of vinylene carbonate additive. Pure Li foils were used as counter electrodes. The discharge-charge measurements were performed on a Neware battery testing system (Shenzhen, China) at the constant current mode in the range of 0.01–2.0 V. The specific capacities were calculated based on the total weight of Si/SiO_x/C nanosheets. The loading weight of active material was fixed at ~1.0 mg cm^{-2}.

RESULTS AND DISCUSSION

Here, we present a very facile and green procedure for obtaining ultrathin Si/SiO_x/C composite nanosheets, as illustrated in Scheme 1. It is found that greenhouse gas CO_2 can readily react with Zintl phase $CaSi_2$ to rapidly separate Si and Ca layers. After removal of the byproduct $CaCO_3$/CaO and mild sonication, the free-standing ultrathin Si/SiO_x/C nanosheets can be produced. As shown in Fig. 1a, the PXRD pattern of the pristine technical grade Zintl $CaSi_2$ shows the presence of silicon impurities. To eliminate the effect of Si impurities (e.g., serving as a capacity contributor) and obtain a deep understanding of the conversion reaction mechanism, it is necessary to remove the crystalline Si impurities before using the pristine $CaSi_2$. In this work, most of the Si impurities were removed from $CaSi_2$ *via* the treatment in 2.0 mol L^{-1} NaOH aqueous solution, as shown in the red curve of Fig. 1a. Meanwhile, the morphology and structure of $CaSi_2$ after NaOH treatment were almost unchanged, as shown in Fig. S1. The NaOH-treated $CaSi_2$ was placed in the center of a tube furnace and reacted with flowing CO_2/Ar (1:4 in volume) gas at

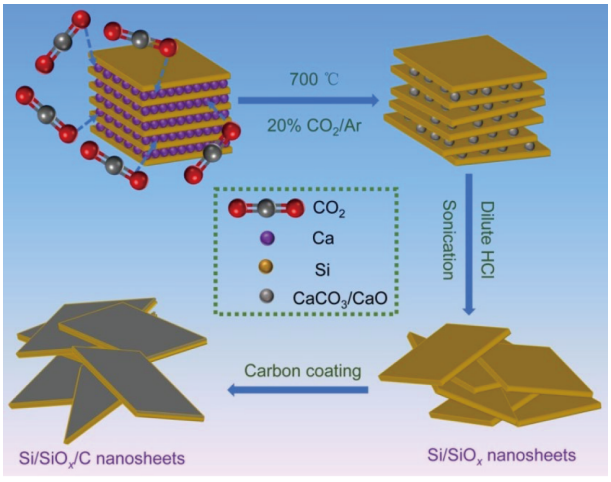

Scheme 1 Schematic illustration of the preparation of the 2D free-standing Si/SiO_x and Si/SiO_x/C nanosheets.

700°C. The $CaSi_2$ precursor readily reacted with CO_2 to produce dark-gray Si/SiO_x nanosheets, CaO, $CaCO_3$ and almost negligible amount of carbon, and the corresponding XRD pattern is shown in Fig. 2b. The coexistence of $CaCO_3$ and CaO could be attributed to the following thermal exfoliation reaction:

$$2CaSi_2 + 2CO_2 \xrightarrow{700^{\circ}C} 4Si + CaO + CaCO_3 + C. \quad (1)$$

Fig. 2a shows the SEM image of the as-prepared (unwashed) Si/SiO_x nanosheets with plate-like structures. The high-resolution TEM (HRTEM) image (Fig. 2d) exhibits three sets of distinct lattice fringes of 0.32, 0.30, and 0.24 nm in accordance with the (111) planes of crystalline cubic Si, (104) planes of hexagonal $CaCO_3$, and the (200) planes of cubic CaO, respectively, which means the byproduct CaO and $CaCO_3$ are included in Si/SiO_x nanosheets before washing. After washing with dilute HCl solution and sonication for 20 min, the 2D free-standing ultrathin Si/SiO_x nanosheets were further exfoliated and purified, as shown in Fig. 2b, thus providing more clearer evidence of the sheet-like structure. The produced free-standing Si/SiO_x nanosheets exhibit ultrathin structures with an average thickness of 8 nm, as shown in Fig. S2.

To further improve the electronic conductivity, the ultrathin Si/SiO_x nanosheets were treated by *in-situ* polydopamine polymerization followed by high-temperature carbonization to form an outer layer of carbon coating. The SEM and TEM images of the carbon-coated $Si/SiO_x/C$ nanosheets are shown in Fig. 2c, e, respectively. Fig. 2c shows that the surface of the as-prepared 2D $Si/SiO_x/C$ nanosheets becomes rougher after the carbon coating. The TEM image in Fig. 2e also reveals the 2D layered structures of $Si/SiO_x/C$ nanosheets. The chemical compositions of $Si/SiO_x/$

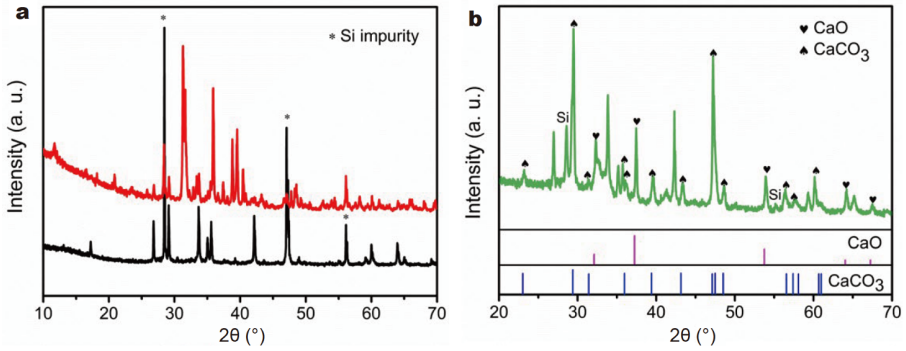

Figure 1 PXRD patterns of (a) the pristine $CaSi_2$ (black curve), and $CaSi_2$ after treated in 2.0 mol L^{-1} NaOH solution (red curve); (b) the as-prepared ultrathin 2D Si/SiO_x nanosheets before HCl washing, as well as the standard PXRD PDF cards of CaO and $CaCO_3$.

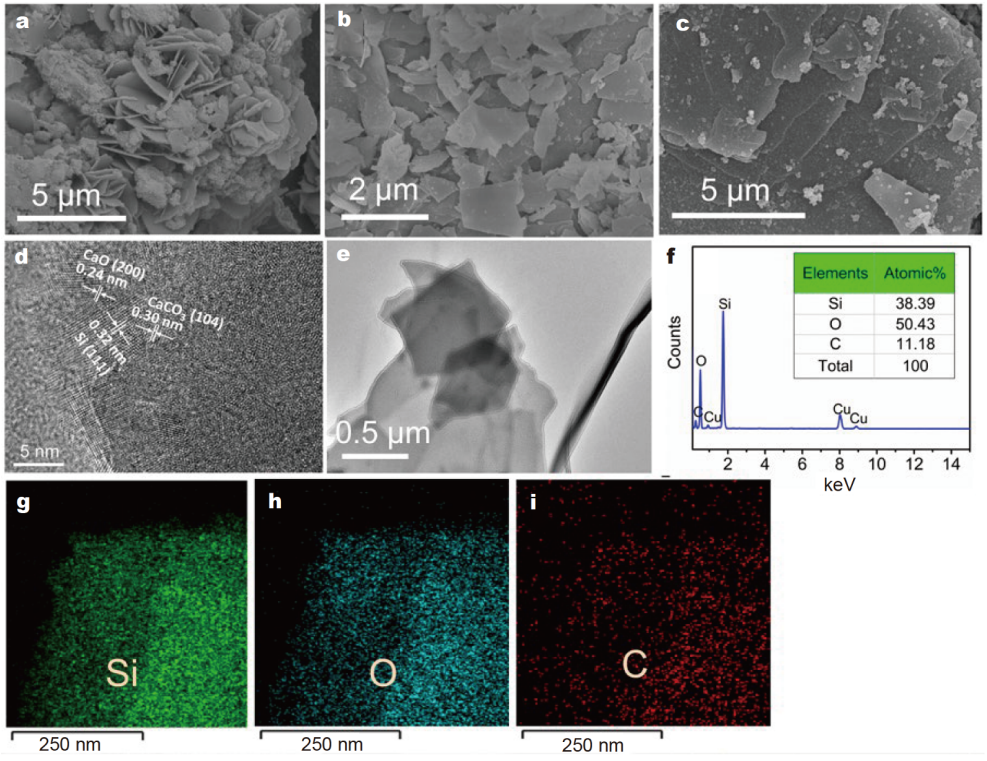

Figure 2 SEM images of (a) the as-prepared 2D Si/SiO_x nanosheets before acid washing, (b) free-standing Si/SiO_x nanosheets after sonication in HCl solution, and (c) $Si/SiO_x/C$ nanosheets after carbon coating. (d) HRTEM image of the Si/SiO_x nanosheets before acid washing and (e) TEM image and (f) EDS spectrum of the $Si/SiO_x/C$ nanosheets. (g–i) The Si, O, and C elemental mappings of the $Si/SiO_x/C$ nanosheets.

C nanosheets were also investigated by EDS, as shown in Fig. 2f. The presence of Si, O, and C elements was confirmed, and no impurities could be detected. Moreover, the elemental mappings clearly demonstrate the homogeneous distribution of Si, O, and C species in the Si/SiO_x/C nanosheets (Fig. 2g–i), implying the uniform coating of outer carbon layer. Moreover, the optical photographs of the product under different reaction stages are shown in Fig. S3. As shown in Fig. S3b, after alkali treatment, the impurity of crystalline Si (Fig. S3a) in the pristine $CaSi_2$ is removed. Afterwards, the color of $CaSi_2$ changes into yellowish-brown after reacting with CO_2, as exhibited in Fig. S3c, d, which can be explained as the formation of Si nanomaterials. After carbon coating , the color of the product turns into light black, as shown in Fig. S3e.

Fig. 3a shows the XRD patterns of Si/SiO_x and Si/SiO_x/C nanosheets, respectively. All of the diffraction peaks centered at 2θ values around 28.5, 47.4, and 56.2° are assigned to the (111), (220), and (311) planes of cubic Si phase, respectively. In addition, after coating with carbon, the XRD pattern of Si/SiO_x/C nanosheets exhibits an obvious wide peak at around 25.2°, corresponding to the (002) planes of partially graphitic carbon outer layer derived from the pyrolysis of polydopamine. Fig. 3b, c show the N_2 adsorption/desorption isotherms and pore size distribution of Si/SiO_x nanosheets, respectively. The Brunauer–Emmett–Teller (BET) surface area of 2D Si/SiO_x nanosheets was measured to be 121.7 $m^2 g^{-1}$ with type IV N_2 adsorption/desorption isotherms, indicating the presence of mesopores in the nanosheet structure. An average pore size of approximately 6.8 nm in diameter was obtained when using the Barrett–Joyner–Halenda (BJH) model to analyze the pore features of the 2D Si/SiO_x nanosheets. The mesopores formed in the 2D Si/SiO_x nanosheets likely result from the templating effect of *in-situ* generated CaO and $CaCO_3$. After coating with thin carbon layers, as shown in Fig. S4, the BET surface area of the Si/SiO_x/C nanosheets is reduced to 79.2 $m^2 g^{-1}$, and no pore structures could be observed, which is mainly ascribed to the filled carbon within pore channels. The XPS survey spectra of the Si/SiO_x nanosheets is illustrated in Fig. S5 with no impurities other than Si, C, and O elements. The Si 2p XPS spectrum of the freshly prepared 2D Si/SiO_x nanosheets shows two main peaks at 99.4 and 103.6 eV, respectively, as shown in Fig. 3d. These two peaks could be further deconvolved into five peaks at 99.4, 100.2, 102.6, 103.6, and 104.5 eV, which correspond to Si (0), Si (+1), Si (+2), Si (+3), and Si (+4) species, respectively [43–46]. The oxidation layer on the Si surface is unavoidable after the sample is exposed to air. Fortunately, an increasing number of investigations have confirmed that the presence of a small amount of SiO_x is beneficial to the electrochemical stability of Si-based anodes [47–55]. After the coating of carbon layer, the Raman spectrum of Si/SiO_x/C nanosheets in Fig. 3e demonstrates the presence of crystalline Si and partially graphitic carbon. The intense peak at approximately 520 cm^{-1} is associated with the Raman signal of crystalline Si. The two peaks located at 1350 and 1590 cm^{-1} correspond to the D band (disordered carbon) and G band (graphitic carbon) of the coated carbon layer, respectively. The calculated intensity I_D/I_G value of Si/SiO_x/C nanosheets is 0.86, suggesting the partial graphitization of carbon, which is consistent with the XRD characterization result. Fig. 3f shows that the weight content of the coated carbon layer in the Si/SiO_x/C nanosheets is ~15 wt%, which is beneficial for achieving a high total specific capacity of the anode.

To investigate the lithium-storage mechanism, the cyclic voltammetry (CV) profiles of Si/SiO_x/C nanosheets electrode during the first three cycles were evaluated at a scanning rate of 0.02 mV s^{-1} (Fig. 4a). In the first discharge process, a weak broad peak was detected between 0.3 and 0.8 V, which was not observed during the following cycles. This lithiation peak could be attributed to the irreversible formation of the solid electrolyte interphase (SEI) film [56,57]. In the first charge process, the peaks located at 0.33 and 0.54 V are ascribed to the delithiation process [58]. In addition, the broad anodic peaks at ~1.2 V is ascribed to the dealloying process of $Li_2Si_2O_5$ [59,60]. This peak

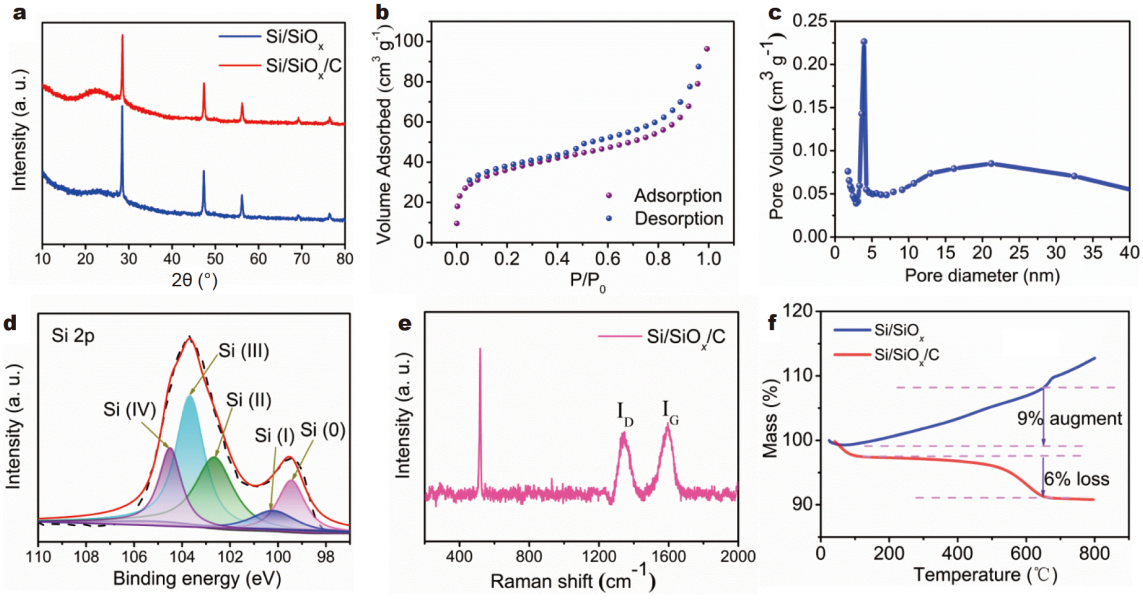

Figure 3 (a) XRD patterns of the ultrathin free-standing Si/SiO_x and Si/SiO_x/C nanosheets, respectively. (b) N_2 sorption-desorption isotherms and (c) pore size distribution of the Si/SiO_x nanosheets. (d) Si 2p XPS spectra of the Si/SiO_x nanosheets. (e) Raman spectrum and (f) TGA curves of the Si/SiO_x and Si/SiO_x/C nanosheets.

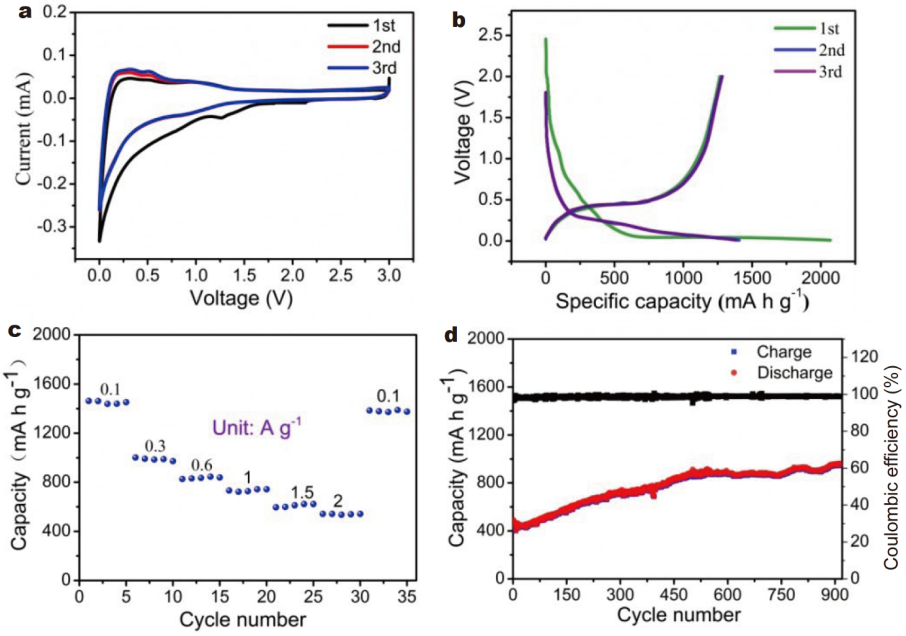

Figure 4 (a) CV curves and (b) charge-discharge curves of the Si/SiO_x/C nanosheets electrode during the first three cycles. (c) Rate performance of the Si/SiO_x/C nanosheets electrode. (d) Long-term cycling stability and the corresponding coulombic efficiency of the Si/SiO_x/C nanosheets electrode at a current density of 0.5 A g^{-1}.

disappears in the following cycles, owing to the irreversible reactions. Furthermore, the CV curves from the 2nd to the 3rd cycle almost overlap, indicating that the Si/SiO_x/C electrode possesses good electrochemical reversibility. Fig. 4b presents the charge-discharge curves of Si/SiO_x/C nanosheets electrode during the initial three cycles at a current density of 0.1 A g^{-1}. The initial specific discharge and charge capacities of the Si/SiO_x/C nanosheets electrode are 2067.2 and 1267.2 mA h g^{-1}, respectively, achieving an initial coulombic efficiency of 61.3%. The capacity loss during the first cycle is mainly attributed to the generation of the SEI film and the irreversible side reaction between SiO_x and the organic electrolyte [61]. Moreover, in the first discharge profile, the existing plateaus between 0.3 and 1.5 V are in accordance with the CV result. After the first cycle, the coulombic efficiency of the Si/SiO_x/C electrode increases to 91% during the second cycle and then rapidly reaches high values over 99% in the subsequent cycles.

Fig. 4c shows the rate performance of the Si/SiO_x/C nanosheets electrode. Before the rate performance test, the electrode was activated at low current densities for 5 cycles. The Si/SiO_x/C nanosheets electrode delivered high specific discharge capacities of 1439, 988, 825, 730, 600, and 541 mA h g^{-1} at the current densities of 0.1, 0.3, 0.6, 1.0, 1.5, and 2.0 A g^{-1}, respectively. The Si/SiO_x/C electrode exhibits good reversibility, and the specific discharge capacity recovered to 1380 mA h g^{-1} when the current density returned to 0.1 A g^{-1} after the charge-discharge cycles at high current densities.

The long-term cycling stability of the Si/SiO_x/C electrode was also evaluated, and the results are shown in Fig. 4d and Fig. S5. During the charge-discharge processes at a small current density of 0.1 A g^{-1}, the Si/SiO_x/C nanosheets electrode shows good electrochemical stability and a high specific capacity of ~1400 mA h g^{-1} even after 200 cycles (Fig. S5). Furthermore, when the current density increases from 0.1 to 0.5 A g^{-1}, the Si/SiO_x/C nanosheets electrode also delivers an ever-increasing specific capacity of ~900 mA h g^{-1} after 920 cycles (Fig. 4d). The phenomenon of increasing capacity could be mainly attributed to the sluggish electrolyte wetting, which is also reported in other studies [62,63]. On the other hand, the cross-sectional SEM images of the Si/SiO_x/C nanosheets electrode also provides solid evidence that the 2D Si/SiO_x/C nanosheets could effectively alleviate the volume variations during the charge-discharge processes. As presented in Fig. S6, the Si/SiO_x/C nanosheets electrode at freshly-prepared status and delithiated status after 500 cycles exhibit negligible changes in electrode thickness. Meanwhile, the SEM image (Fig. S7) of the Si/SiO_x/C nanosheets electrode after 500 cycles (washed with acetonitrile to remove the SEI layer before SEM measurements) also reveals that the 2D structures of Si/SiO_x/C nanosheets could be maintained even after deep charging-discharging cycles.

In contrast to the high cycling stability of the Si/SiO_x/C nanosheets electrode, the Si/SiO_x nanosheets electrode without carbon coating displays rapid capacity fading due to the relatively poor conductivity. As shown in Fig. S8, after merely a few cycles, the discharge capacity of the Si/SiO_x nanosheets electrode decreases to almost zero. The Nyquist plots of the Si/SiO_x and Si/SiO_x/C nanosheets electrodes measured by electrochemical impedance spectroscopy (EIS) based on a three-electrode test system are presented in Fig. 5. The main difference in the Nyquist plots of these two electrodes is presented in the two distinct semicircles in the high-frequency regions. Apparently, after the carbon coating, the Si/SiO_x/C nanosheets electrode exhibits significantly lower resistance than the Si/SiO_x nanosheets electrode, indicating that the conductive coating on the Si/SiO_x nanosheets can greatly improve the electroconductivity and cycling stability.

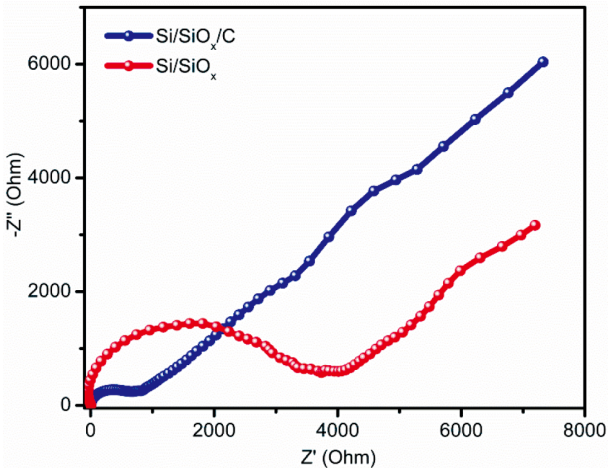

Figure 5 EIS curves of the Si/SiO_x and $Si/SiO_x/C$ nanosheets electrodes.

CONCLUSIONS

In summary, here we propose a convenient and environmentally friendly method to prepare 2D free-standing $Si/SiO_x/C$ nanosheets with ultrathin thicknesses in a batch scale. The exfoliation reaction of $CaSi_2$ in CO_2 atmosphere could produce ultrathin Si/SiO_x nanosheets and *in situ* generate the side products of $CaCO_3$ and CaO. During the following sonication in HCl solution, free-standing Si/SiO_x nanosheets could be easily produced with a high yield. After carbon coating, the 2D $Si/SiO_x/C$ nanosheets were produced, which exhibited high capacity and excellent cycling stability when serving as anode material in LIBs. The reversible specific capacity was as high as ~1400 mA h g^{-1} even after 200 cycles at 0.1 A g^{-1}. The discharge capacity can maintain at ~900 mA h g^{-1} even after charging-discharging at 0.5 A g^{-1} for 920 cycles, indicating the remarkable cycling stability. We expect that this work will provide new insights and inspirations to rationally design and fabricate low-dimensional Si-based anode materials for high-performance LIBs.

Received 25 March 2021; accepted 17 May 2021; published online 9 July 2021

1 Liang G, Yang L, Han Q, *et al.* Conductive $Li_{3.08}Cr_{0.02}Si_{0.09}V_{0.9}O_4$ anode material: Novel "zero-strain" characteristic and superior electrochemical Li^+ storage. Adv Energy Mater, 2020, 10: 1904267
2 Xiao Z, Lei C, Yu C, *et al.* Si@Si_3N_4@C composite with egg-like structure as high-performance anode material for lithium ion batteries. Energy Storage Mater, 2020, 24: 565–573
3 Li J, Han L, Li Y, *et al.* MXene-decorated SnS_2/Sn_3S_4 hybrid as anode material for high-rate lithium-ion batteries. Chem Eng J, 2020, 380: 122590
4 Chang X, Xie Z, Liu Z, *et al.* Aluminum: An underappreciated anode material for lithium-ion batteries. Energy Storage Mater, 2020, 25: 93–99
5 Sahu SR, Rikka VR, Haridoss P, *et al.* A novel α-MoO_3/single-walled carbon nanohorns composite as high-performance anode material for fast-charging lithium-ion battery. Adv Energy Mater, 2020, 10: 2001627
6 Xiao Z, Yu C, Lin X, *et al.* TiO_2 as a multifunction coating layer to enhance the electrochemical performance of SiO_x@TiO_2@C composite as anode material. Nano Energy, 2020, 77: 105082
7 Chan CK, Peng H, Liu G, *et al.* High-performance lithium battery anodes using silicon nanowires. Nat Nanotech, 2008, 3: 31–35
8 Wu H, Chan G, Choi JW, *et al.* Stable cycling of double-walled silicon nanotube battery anodes through solid–electrolyte interphase control. Nat Nanotech, 2012, 7: 310–315
9 Rahman MA, Song G, Bhatt AI, *et al.* Nanostructured silicon anodes for high-performance lithium-ion batteries. Adv Funct Mater, 2016, 26: 647–678
10 An Y, Fei H, Zeng G, *et al.* Green, scalable, and controllable fabrication of nanoporous silicon from commercial alloy precursors for high-energy lithium-ion batteries. ACS Nano, 2018, 12: 4993–5002
11 Rodrigues MTF, Babu G, Gullapalli H, *et al.* A materials perspective on Li-ion batteries at extreme temperatures. Nat Energy, 2017, 2: 17108
12 Lu J, Wu T, Amine K. State-of-the-art characterization techniques for advanced lithium-ion batteries. Nat Energy, 2017, 2: 17011
13 Novoselov KS, Geim AK, Morozov SV, *et al.* Electric field effect in atomically thin carbon films. Science, 2004, 306: 666–669
14 Novoselov KS, Geim AK, Morozov SV, *et al.* Two-dimensional gas of massless Dirac fermions in graphene. Nature, 2005, 438: 197–200
15 Geim AK, Novoselov KS. The rise of graphene. Nat Mater, 2007, 6: 183–191
16 Wang QH, Kalantar-Zadeh K, Kis A, *et al.* Electronics and optoelectronics of two-dimensional transition metal dichalcogenides. Nat Nanotech, 2012, 7: 699–712
17 Manzeli S, Ovchinnikov D, Pasquier D, *et al.* 2D transition metal dichalcogenides. Nat Rev Mater, 2017, 2: 17033
18 Tang L, Li T, Luo Y, *et al.* Vertical chemical vapor deposition growth of highly uniform 2D transition metal dichalcogenides. ACS Nano, 2020, 14: 4646–4653
19 Fu Q, Han J, Wang X, *et al.* 2D transition metal dichalcogenides: Design, modulation, and challenges in electrocatalysis. Adv Mater, 2021, 33: 2170045
20 Anasori B, Lukatskaya MR, Gogotsi Y. 2D metal carbides and nitrides (MXenes) for energy storage. Nat Rev Mater, 2017, 2: 16098
21 Naguib M, Mashtalir O, Carle J, *et al.* Two-dimensional transition metal carbides. ACS Nano, 2012, 6: 1322–1331
22 Tan TL, Jin HM, Sullivan MB, *et al.* High-throughput survey of ordering configurations in MXene alloys across compositions and temperatures. ACS Nano, 2017, 11: 4407–4418
23 Ghidiu M, Lukatskaya MR, Zhao MQ, *et al.* Conductive two-dimensional titanium carbide 'clay' with high volumetric capacitance. Nature, 2014, 516: 78–81
24 Gu J, Zhu Q, Shi Y, *et al.* Single zinc atoms immobilized on MXene ($Ti_3C_2Cl_x$) layers toward dendrite-free lithium metal anodes. ACS Nano, 2020, 14: 891–898
25 Wu X, Ge R, Chen PA, *et al.* Thinnest nonvolatile memory based on monolayer h-BN. Adv Mater, 2019, 31: 1806790
26 Weng Q, Wang X, Wang X, *et al.* Functionalized hexagonal boron nitride nanomaterials: Emerging properties and applications. Chem Soc Rev, 2016, 45: 3989–4012
27 Huang Y, Chen B, Duan J, *et al.* Graphitic carbon nitride (g-C_3N_4): An interface enabler for solid-state lithium metal batteries. Angew Chem Int Ed, 2020, 59: 3699–3704
28 Deng Y, Liu J, Huang Y, *et al.* Engineering the photocatalytic behaviors of g/C_3N_4-based metal-free materials for degradation of a representative antibiotic. Adv Funct Mater, 2020, 30: 2002353
29 Patnaik S, Sahoo DP, Parida K. Recent advances in anion doped g-C_3N_4 photocatalysts: A review. Carbon, 2021, 172: 682–711
30 Tang J, Yin Q, Wang Q, *et al.* Two-dimensional porous silicon nanosheets as anode materials for high performance lithium-ion batteries. Nanoscale, 2019, 11: 10984–10991
31 Xu K, Ben L, Li H, *et al.* Silicon-based nanosheets synthesized by a topochemical reaction for use as anodes for lithium ion batteries. Nano Res, 2015, 8: 2654–2662
32 Yue XY, Abulikemu A, Li XL, *et al.* Vermiculite derived porous silicon nanosheet as a scalable and low cost anode material for lithium-ion batteries. J Power Sources, 2019, 410-411: 132–136
33 Ryu J, Hong D, Choi S, *et al.* Synthesis of ultrathin Si nanosheets from natural clays for lithium-ion battery anodes. ACS Nano, 2016, 10: 2843–2851
34 Yu X, Xue F, Huang H, *et al.* Synthesis and electrochemical properties of silicon nanosheets by DC arc discharge for lithium-ion batteries. Nanoscale, 2014, 6: 6860–6865

35 Kim WS, Hwa Y, Shin JH, *et al.* Scalable synthesis of silicon nanosheets from sand as an anode for Li-ion batteries. Nanoscale, 2014, 6: 4297–4302
36 Chen S, Chen Z, Xu X, *et al.* Scalable 2D mesoporous silicon nanosheets for high-performance lithium-ion battery anode. Small, 2018, 14: 1703361
37 Wang H, Tang W, Ni L, *et al.* Synthesis of silicon nanosheets from kaolinite as a high-performance anode material for lithium-ion batteries. J Phys Chem Solids, 2020, 137: 109227
38 An Y, Tian Y, Wei C, *et al.* Scalable and physical synthesis of 2D silicon from bulk layered alloy for lithium-ion batteries and lithium metal batteries. ACS Nano, 2019, 13: 13690–13701
39 Ko M, Chae S, Ma J, *et al.* Scalable synthesis of silicon-nanolayer-embedded graphite for high-energy lithium-ion batteries. Nat Energy, 2016, 1: 16113
40 Gu J, Du Z, Zhang C, *et al.* Liquid-phase exfoliated metallic antimony nanosheets toward high volumetric sodium storage. Adv Energy Mater, 2017, 7: 1700447
41 Kumai Y, Shirai S, Sudo E, *et al.* Characteristics and structural change of layered polysilane (Si_6H_6) anode for lithium ion batteries. J Power Sources, 2011, 196: 1503–1507
42 Sun L, Su T, Xu L, *et al.* Two-dimensional ultra-thin SiO_x ($0 < x < 2$) nanosheets with long-term cycling stability as lithium ion battery anodes. Chem Commun, 2016, 52: 4341–4344
43 Shallenberger JR. Determination of chemistry and microstructure in SiO_x ($0.1 < x < 0.8$) films by X-ray photoelectron spectroscopy. J Vacuum Sci Tech A-Vacuum Surfs Films, 1996, 14: 693–698
44 Ulusoy Ghobadi TG, Ghobadi A, Okyay T, *et al.* Controlling luminescent silicon nanoparticle emission produced by nanosecond pulsed laser ablation: role of interface defect states and crystallinity phase. RSC Adv, 2016, 6: 112520
45 Ntais S, Dracopoulos V, Siokou A. $TiCl_4(THF)_2$ impregnation on a flat SiO_x/Si(100) and on polycrystalline Au foil: determination of surface species using XPS. J Mol Catal A-Chem, 2004, 220: 199–205
46 Xun S, Song X, Grass ME, *et al.* Improved initial performance of Si nanoparticles by surface oxide reduction for lithium-ion battery application. Electrochem Solid-State Lett, 2011, 14: A61
47 Xue H, Wu Y, Zou Y, *et al.* Unraveling metal oxide role in exfoliating graphite: new strategy to construct high-performance graphene-modified SiO_x-based anode for lithium-ion batteries. Adv Funct Mater, 2020, 30: 1910657
48 Su A, Li J, Dong J, *et al.* An amorphous/crystalline incorporated Si/SiO_x anode material derived from biomass corn leaves for lithium-ion batteries. Small, 2020, 16: 2001714
49 Li G, Huang LB, Yan MY, *et al.* An integral interface with dynamically stable evolution on micron-sized SiO_x particle anode. Nano Energy, 2020, 74: 104890
50 Jiang Y, Liu S, Ding Y, *et al.* Modification based on primary particle level to improve the electrochemical performance of SiO-based anode materials. J Power Sources, 2020, 467: 228301
51 Yan MY, Li G, Zhang J, *et al.* Enabling SiO_x/C anode with high initial coulombic efficiency through a chemical pre-lithiation strategy for high-energy-density lithium-ion batteries. ACS Appl Mater Interfaces, 2020, 12: 27202–27209
52 Li G, Li JY, Yue FS, *et al.* Reducing the volume deformation of high capacity SiO_x/G/C anode toward industrial application in high energy density lithium-ion batteries. Nano Energy, 2019, 60: 485–492
53 Lee J, Moon J, Han SA, *et al.* Everlasting living and breathing gyroid 3D network in Si@SiO_x/C nanoarchitecture for lithium ion battery. ACS Nano, 2019, 13: 9607–9619
54 Han M, Yu J. Subnanoscopically and homogeneously dispersed SiO_x/C composite spheres for high-performance lithium ion battery anodes. J Power Sources, 2019, 414: 435–443
55 Xu Q, Sun JK, Yin YX, *et al.* Facile synthesis of blocky SiO_x/C with graphite-like structure for high-performance lithium-ion battery anodes. Adv Funct Mater, 2018, 28: 1705235
56 Li Z, Zhao H, Wang J, *et al.* Rational structure design to realize high-performance SiO_x@C anode material for lithium ion batteries. Nano Res, 2020, 13: 527–532
57 Lin J, Peng H, Kim JH, *et al.* Lithium fluoride coated silicon nanocolumns as anodes for lithium ion batteries. ACS Appl Mater Interfaces, 2020, 12: 18465–18472
58 Shi J, Zu L, Gao H, *et al.* Silicon-based self-assemblies for high volumetric capacity Li-ion batteries *via* effective stress management. Adv Funct Mater, 2020, 30: 2002980
59 Carroll GM, Schulze MC, Martin TR, *et al.* SiO_2 is wasted space in single-nanometer-scale silicon nanoparticle-based composite anodes for Li-ion electrochemical energy storage. ACS Appl Energy Mater, 2020, 3: 10993–11001
60 Sun Q, Zhang B, Fu ZW. Lithium electrochemistry of SiO_2 thin film electrode for lithium-ion batteries. Appl Surf Sci, 2008, 254: 3774–3779
61 Yu Q, Ge P, Liu Z, *et al.* Ultrafine SiO_x/C nanospheres and their pomegranate-like assemblies for high-performance lithium storage. J Mater Chem A, 2018, 6: 14903–14909
62 An Y, Tian Y, Zhang Y, *et al.* Two-dimensional silicon/carbon from commercial alloy and CO_2 for lithium storage and flexible $Ti_3C_2T_x$ MXene-based lithium–metal batteries. ACS Nano, 2020, 14: 17574–17588
63 Lin H, Qiu W, Liu J, *et al.* Silicene: Wet-chemical exfoliation synthesis and biodegradable tumor nanomedicine. Adv Mater, 2019, 31: 1903013

Acknowledgements This work was financially supported by the National Key Research and Development Program of China (2017YFA0208200 and 2016YFB0700600), the Fundamental Research Funds for the Central Universities of China (0205-14380219), the Projects of National Natural Science Foundation of China (22022505, 21872069 and 51761135104), the Natural Science Foundation of Jiangsu Province (BK20181056, BK20180008 and BK20191042), Jiangsu Postdoctoral Science Fundation (2020Z258), and the Funding for School-level Research Projects of Yancheng Institute of Technology (xjr2019006).

Author contributions Sun L and Jin Z conceived and designed the study; Sun L, Xie J and Huang S performed the synthesis and electrochemical test; Liu Y and Zhang L performed the SEM and TEM measurements; Wu J contributed to the reaction mechanism analysis. The manuscript was written through contributions of all authors. All authors have given approval to the final version of the manuscript.

Conflict of interest The authors declare no conflict of interest.

Supplementary information Supporting data are available in the online version of the paper.

Lin Sun received his MSc degree in chemical engineering, from the School of Petrochemical Engineering, Changzhou University. He obtained the PhD degree in chemistry from Nanjing University. His research interests are focused on organic/inorganic porous materials for adsorption, separation, catalysis, optoelectronics, and energy science by using new synthetic methods and strategies under the guidance of modern computational chemistry.

Zhong Jin received his BSc (2003) and PhD (2008) in chemistry from Peking University. He worked as a postdoctoral scholar at Rice University and Massachusetts Institute of Technology. Now he is a professor at the School of Chemistry and Chemical Engineering, Nanjing University. He leads a research group on functional nanomaterials and devices for energy conversion and storage.

二氧化碳快速剥离Zintl相硅化钙制备超薄Si/SiO$_x$/C纳米片及其高效储锂性能

孙林[1,2*], 谢杰[1], 黄松超[1], 刘宴秀[1], 张磊[1], 吴俊[1], 金钟[1,2*]

摘要 半导体硅(Si)纳米材料在电子、物理、储能等领域有着广阔的应用前景. 然而, 到目前为止, 由于一些长期存在的难题, 如制备工艺复杂, 时间、能耗较大等, 通过高效低成本的途径实现纳米硅材料的规模化生产依然具有挑战. 在本工作中, 我们报道了一种绿色、廉价的纳米Si材料的制备方法: 通过CO_2快速热剥离层状Zintl相化合物$CaSi_2$高产率地制备二维超薄Si/SiO$_x$纳米片. 我们发现$CaSi_2$可以在一定条件下和CO_2稳定反应. 利用此特性并借助温和超声处理, 可以高产量制备出超薄Si/SiO$_x$纳米片. 通过导电化处理, 得到Si/SiO$_x$/C复合纳米片. 该复合材料作为锂离子电池的负极材料, 具有较高的可逆容量和优异的电化学稳定性. 我们希望本研究能为批量生产高容量锂离子电池的硅基纳米结构材料提供新的思路.